Radiography Open

ISSN: 2387-3345 Vol 12, No 1 (2026) https://doi.org/10.7577/radopen.6648

Design and Validation of a Cellulose Nanofiber-based Phantom for Modeling Extracellular Water Diffusion

Kazuya Sakoda[1], Shogo Baba[2]

[1] Department of Radiological Technology, Kagoshima Medical Technology College, Kagoshima, Japan

[2] Information Technology Center, Seinan Gakuin University, Fukuoka, Japan

*Corresponding author: Kazuya Sakoda rt.sakoda@harada-gakuen.ac.jp

Abstract

Introduction: The current study aimed to develop a novel diffusion phantom composed of cellulose nanofiber (CNF) and glass beads (GBs), and evaluate its validation for quantitative diffusion-weighted imaging (DWI) using short-term apparent diffusion coefficient (ADC) stability and microstructural correlation.

Methods: A cross-sectional, A series of phantoms were prepared by mixing CNF with varying amounts of GBs. Seven phantoms with GB concentrations ranging from 0 to 8.4 g per 30 ml were scanned on a 3.0 T MRI at days 0, 30, 60, and 90 using a single-shot EPI DWI (b = 0, 1000 s/mm²).

Results: ADC and CV values were derived. A strong negative correlation was observed between GB density and ADC ($r = –0.998$, $p < 0.001$). CVs remained below 5% for all GB concentrations except the highest (8.4 g), indicating excellent stability.

Conclusion: The CNF based phantom offers a stable model for simulating restricted diffusion, overcoming drawbacks of existing phantoms. Its performance may support future applications in DWI protocol standardization and preliminary validation of quantitative ADC measurements.

©2026 the author(s). This is an Open Access article distributed under the terms of the Creative Commons Attribution 4.0 International License (http://creativecommons.org/licenses/by/4.0/), allowing third parties to copy and redistribute the material in any medium or format and to remix, transform, and build upon the material for any purpose, even commercially, provided the original work is properly cited and states its license.

Introduction

Diffusion-weighted imaging (DWI) is an MRI technique that sensitively detects the microscopic movement of water molecules within biological tissues. It primarily produces image contrast based on the diffusion behavior of water molecules in the extracellular space, allowing for the sensitive identification of alterations in cell density and the structure of the extracellular matrix.[1, 2] In DWI, motion probing gradients (MPGs) are symmetrically applied before and after the 180° refocusing pulse in a spin-echo sequence. The degree of diffusion weighting, indicated by the b-value, is determined by adjusting the gradient strength, the duration of gradient application, and the interval between gradient pulses. The apparent diffusion coefficient (ADC) is then derived from DWI data acquired using two or more different b-values. As a quantitative marker of cellularity, the ADC is widely used in tumor grading and various diagnostic assessments.[3-6]

DWI phantoms support the assessment of model-specific bias and uncertainty in quantitative diffusion metrics, enabling the distinction between noise-related artifacts and inherent tissue properties, while also contributing to the development of quantitative DWI techniques. Traditionally, these phantoms have utilized substances such as sucrose,[7, 8] alkanes,[9, 10] or polyvinylpyrrolidone (PVP),[11, 12] where ADC values are controlled by modifying solution viscosity without introducing structural barriers to diffusion. In contrast, ADC reductions in biological tissues are affected not only by viscosity but also by factors like the intracellular and extracellular environments and microperfusion. As a result, there is significant interest in developing phantoms that more accurately mimic these complex physiological conditions. Materials such as glass beads (GBs)[13, 14] and acrylic fine particles[15] have been used to model extracellular water diffusion in DWI phantoms. To construct such models, preventing bead aggregation and sedimentation in the solution is crucial. Previous approaches to address this include embedding the beads in agarose to form a gel matrix that minimizes settling,[13, 14] or using neutral detergents with agitation just prior to imaging, followed by acquisition within a brief timeframe.[15] However, the gelation method may still allow bead settling before solidification completes, while the detergent-based method may result in bead movement during imaging. Although matching the specific gravities of the beads and surrounding medium has been proposed,[16] this often leads to increased solution viscosity, hindering accurate replication of extracellular diffusion coefficients. Therefore, a different approach is necessary for creating a stable bead-based phantom.

Cellulose nanofiber (CNF) is a material obtained from plant-derived cellulose fibers that have been broken down and refined to the nanometer scale.[17] Although naturally sourced and environmentally sustainable, CNF possesses an exceptional set of characteristics: it is one-fifth the weight of steel while being five times stronger, has low thermal expansion, and exhibits high water absorbency. Furthermore, because it is derived from renewable plant materials, CNF is widely available and can be sourced from familiar, sustainable origins. A key property of CNF is its effectiveness as a dispersant, capable of keeping fine particles—

such as diamond powder—evenly distributed over long durations.[18] This capability prevents both sedimentation and aggregation, improving the homogeneity and stability of particle suspensions across various uses. Based on these distinctive dispersive characteristics, we hypothesized that CNF could be used to develop a new DWI phantom incorporating microspheres. This study aimed to create a CNF-based DWI phantom embedded with GBs and to evaluate the short-term stability of its ADC values over a 3-month period.

Materials and methods

MR Scanner

A 3.0-T MRI system (Achieva dStream, Philips Healthcare, Best, Netherlands) equipped with a 32-channel head-neck coil was used for this study. All images were acquired in the coronal plane.

Phantom Study

Biomass nanofiber BiNFi-s (2 wt%, CNF WFo-10002, purity >99.5%) was sourced from Sugino Machine Co., Ltd. (Toyama, Japan, https://www.sugino.com/), and soda-lime GBs (P2015SL-2.5, nominal diameter 10 μm, with over 95% of particles within the specified range; particle density 2.5 g/cm^3) were procured from Cospheric LLC (https://www.cospheric.com/). A series of phantoms were created by blending CNF with different concentrations of GBs. The GB content per 30 ml phantom was set at 0, 1.4, 2.8, 4.2, 5.6, 7.0, and 8.4 g (Figure 1). The phantom containing 0 g/30 ml of GBs was included as a CNF-only internal reference to evaluate the baseline diffusion property of the CNF suspension. No independent pure-water reference phantom was scanned. To achieve a uniform dispersion of GBs within the CNF medium, each mixture was stirred at 1,000 rpm for 10 min using a magnetic stirrer (RCH-1000, Tokyo Rikakikai Co., Ltd.). After stirring, each mixture was transferred into a 50-ml plastic tube. The samples were degassed using a BACOENG 12 L vacuum degassing chamber to remove macroscopic air bubbles. Each phantom was fixed to the bottom of the container using double-sided adhesive tape to minimize mechanical displacement. The phantoms were left undisturbed in the MRI room maintained at 24°C for 24 h before imaging. Each phantom was subsequently placed at the isocenter of the static magnetic field and allowed to reach thermal equilibrium for 30 min before scanning. T2 value measurements and DWI were then conducted. DWI acquisitions were performed seven times. To assess short-term stability, the identical imaging protocol was repeated on days 30, 60, and 90.

T2 measurements were obtained using a multiple spin echo sequence with 16 echo times (TE) (15–240 ms, 15 ms spacing) and the following parameters: repetition time (TR) = 5,000 ms; bandwidth =106.8 Hz/pixel; field of view (FOV) = 220 mm; 152 × 105; slice thickness = 4 mm; number of slices = 1; total acquisition time = 16 min and 8 s. DWI was performed using a vendor-provided clinical single-shot echo planar imaging sequence with the following parameters: TR = 5,000 ms; TE = 56.1 ms (minimum); bandwidth = 2,572.9 Hz/pixel; FOV = 180 mm; matrix size = 92 × 87; slice thickness = 7 mm; number of slices = 7; MPG direction = 3; b-values = 0 and 1,000 s/mm^2; and total acquisition time = 1 min and 2 s. The diffusion

gradient duration (δ) and diffusion gradient separation (Δ) were not directly accessible from the clinical scanner interface or the exported imaging protocol and therefore could not be reported.

T2 maps were generated by fitting the acquired signal intensities to an exponential decay curve. ADC maps were computed on a pixel-by-pixel basis using the Stejskal–Tanner equation with the b_0 and b_{1000} images. Both T2 and ADC maps were created using the scanner's built-in software. No additional denoising, Gibbs-ringing correction, motion correction, or susceptibility-distortion correction was applied. After map generation, region of interest (ROI) analysis was conducted using ImageJ software (version 1.8.0_322, National Institute of Health, Bethesda, Maryland, USA). Circular ROIs were placed in the central region of each phantom, and the corresponding T2 and ADC values were quantitatively assessed within these areas.

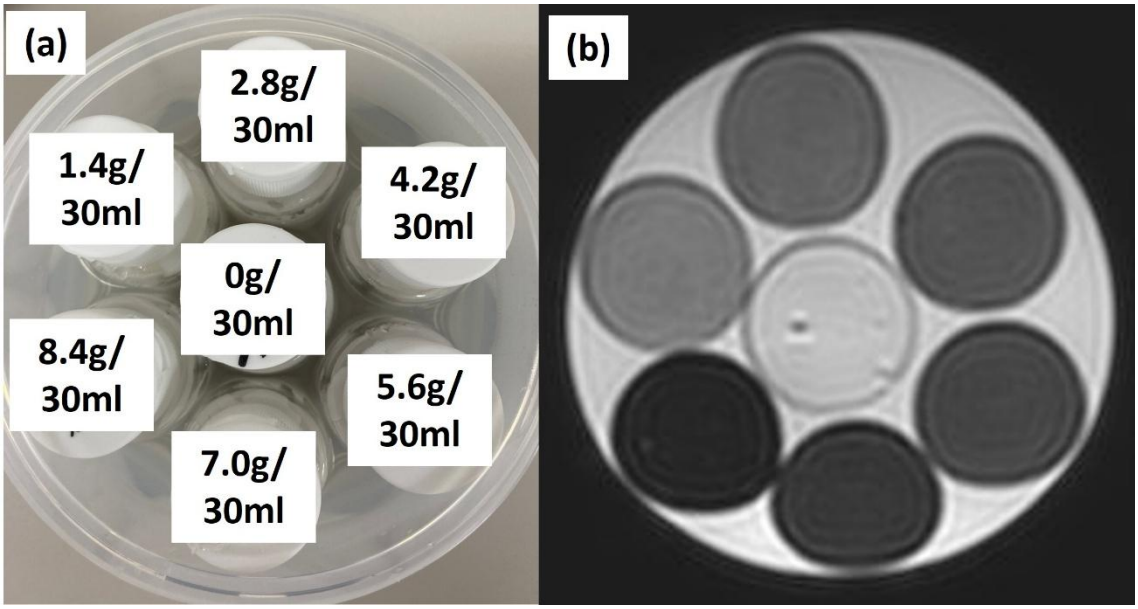

Figure 1. Theoretical value of the GB Density Within the Phantom

First, the weight (g) of a single glass bead (GB) was calculated using the following equation:

Weight of a single GB (g) = (4/3) × π × (radius of GB) ³ × (specific gravity of GB)

The number of GBs per gram was then obtained as the reciprocal of the weight of a single GB.

Because the total volume of each phantom was adjusted to 30 cm³, the GB density was calculated as follows:

GB density (counts per cm³) = (amount of GB in the phantom [g]) / (weight of a single GB × 30)

Using this formula, the GB density of each phantom was determined.

Statistical Analysis

The Shapiro–Wilk test was used to evaluate the normality of the ADC values. Data are reported as mean $\pm$ standard deviation (SD).

Pearson's correlation coefficient was used to evaluate the relationship between GB density and ADC values. Inter-day variability of ADC measurements for each phantom was evaluated by calculating the coefficient of variation (CV), using the formula: CV (%) = (SD of ADC/mean ADC) $\times$ 100. Based on prior studies, a CV <5% was considered acceptable.[10, 19, 20]

All statistical analyses were performed using GraphPad Prism 10.4.2 (GraphPad Prism, San Diego, CA, USA). A p-value of <0.05 was considered statistically significant.

Results

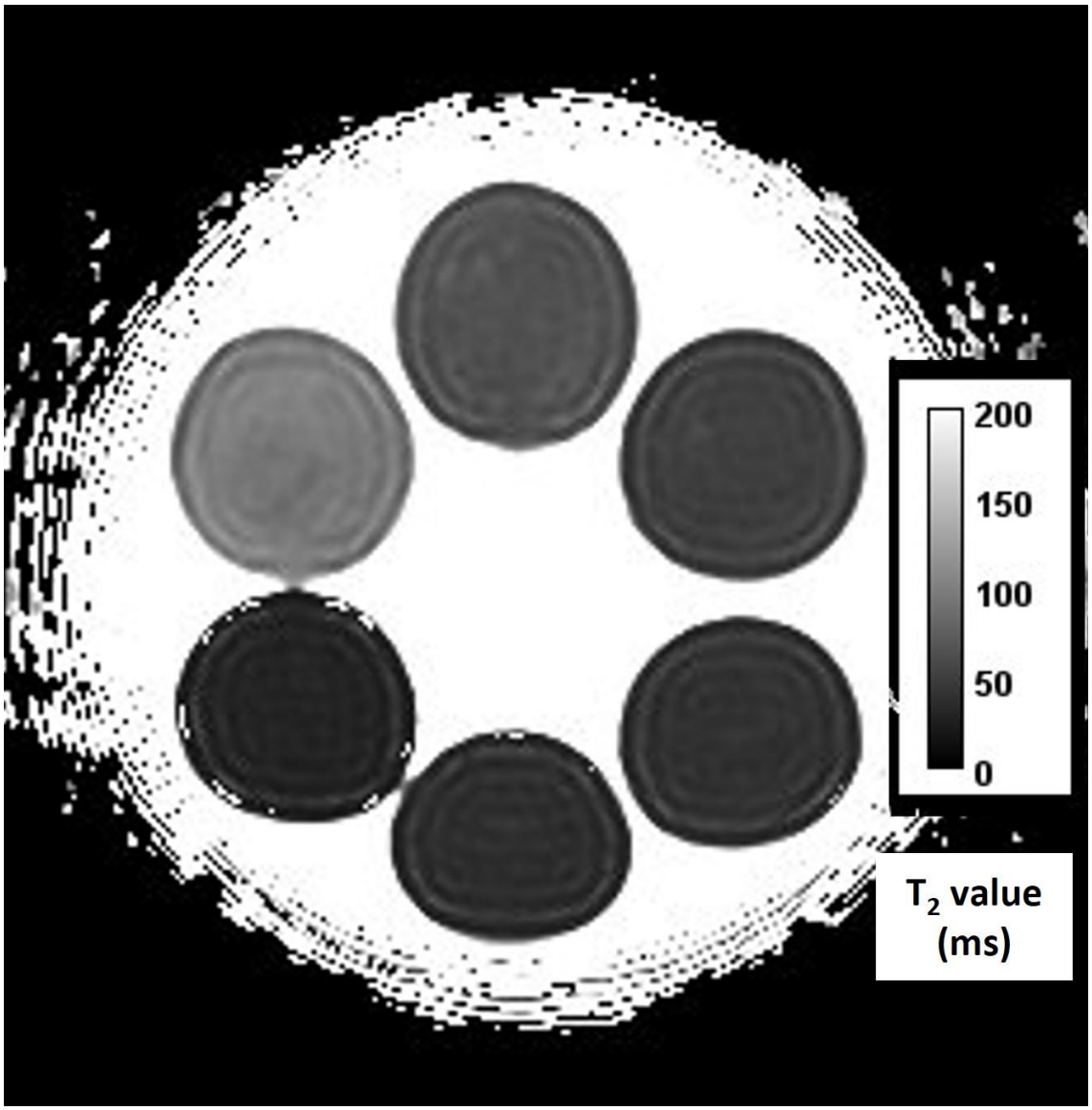

Figure 2. T2 maps of the phantoms used in this study

Figure 2 presents the T2 maps. The measured T2 values for the phantoms containing 0, 1.4, 2.8, 4.2, 5.6, 7.0, and 8.4 g of GB per 30 ml were 353.6, 87.6, 64.5, 49.2, 38.7, 35.5, and 27.5 ms, respectively. The corresponding GB densities (counts per $cm^3 \times 10^8$) were 0, 0.36, 0.71, 1.07, 1.43, 1.78 and 2.14, respectively.

A strong negative correlation was identified between GB density and ADC values, with a Pearson's correlation coefficient of −0.9977 (p = 0.0004) (Figure 3).

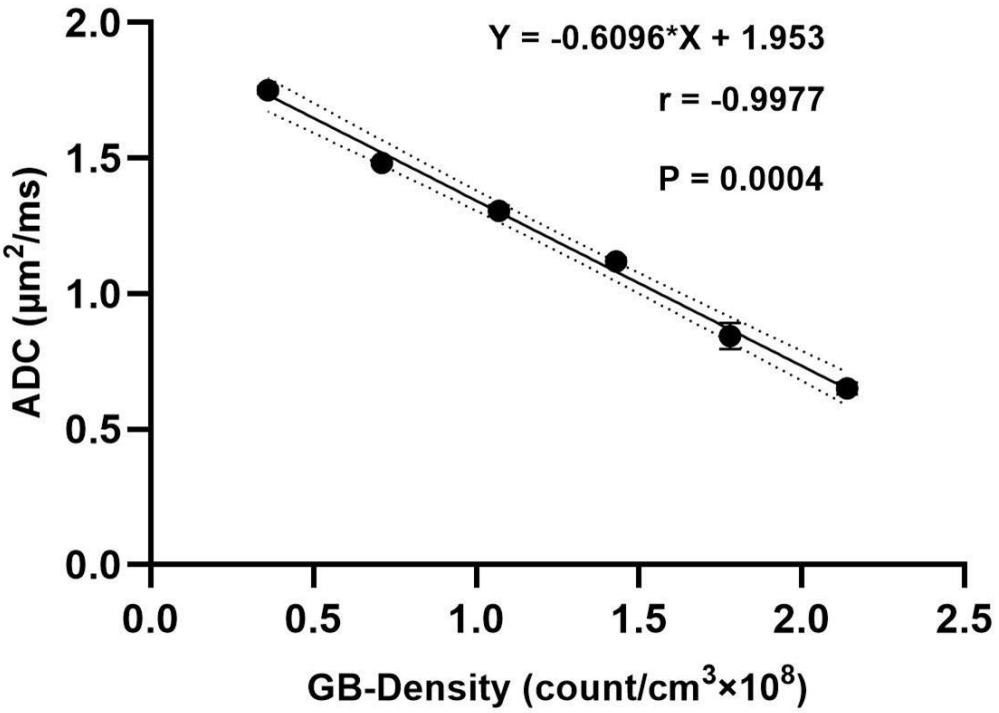

Figure 3. Relationship between glass bead density, as determined from microscopic analysis, and apparent diffusion coefficient values. A strong negative correlation was identified (Pearson's correlation coefficient = −0.9977, p = 0.0004)

The ADC map obtained from imaging on day 0 is shown in Figure 4 and the ADC values recorded on days 0, 30, 60, and 90 are summarized in Table 1. The calculated CVs for each phantom were as follows: 0 g per 30 ml, 0.51%; 1.4 g per 30 ml, 0.92%; 2.8 g per 30 ml, 1.19%; 4.2 g per 30 ml, 1.89%; 5.6 g per 30 ml, 4.22%; 7.0 g per 30 ml, 4.73%; and 8.4 g per 30 ml, 7.78%. All phantoms except the one containing 8.4 g per 30 ml of GB exhibited CVs below 5%, demonstrating excellent short-term stability of ADC measurements across the 90-day study period.

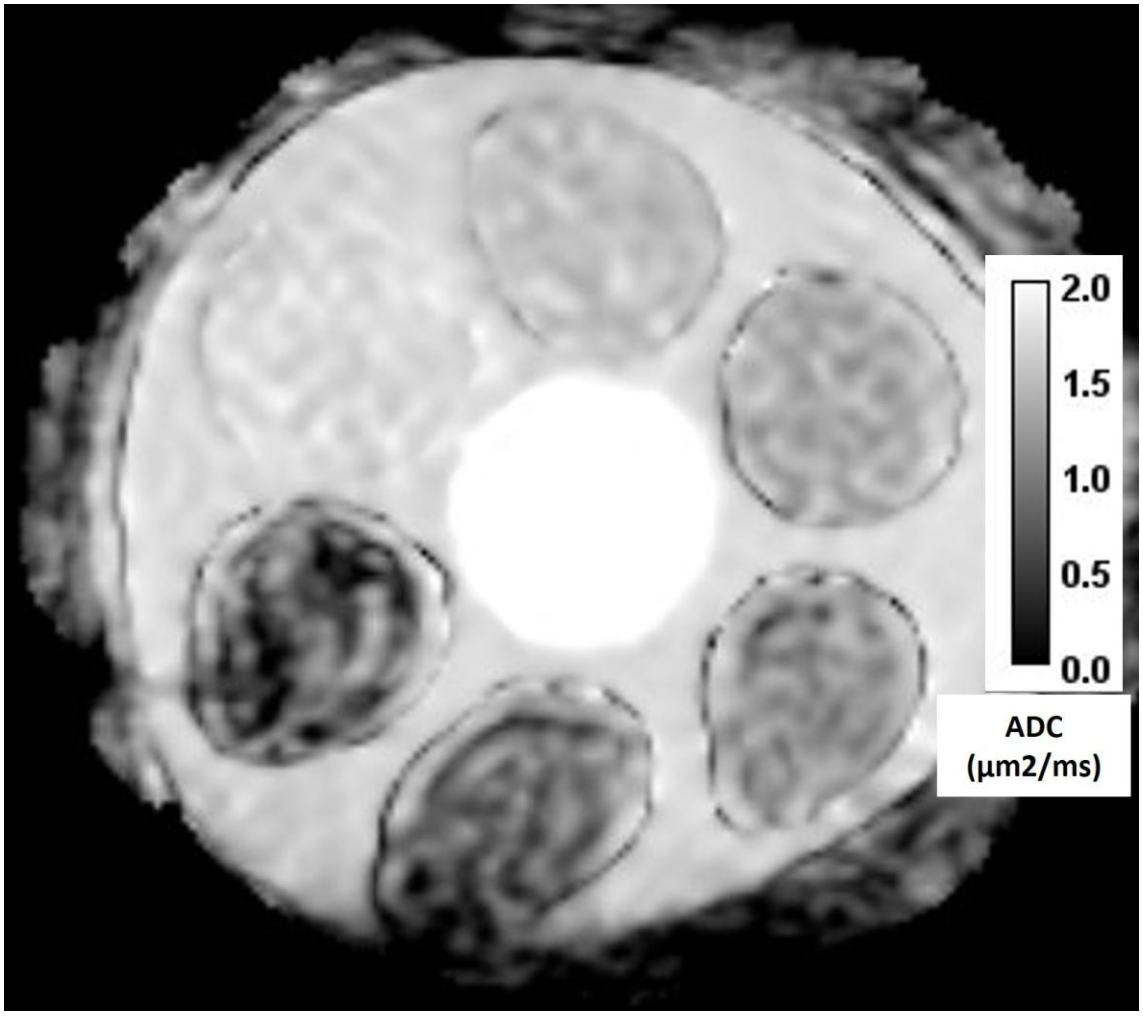

Figure 4. Apparent diffusion coefficient maps of the phantom used in this study

Table 1. Apparent diffusion coefficient (ADC) values corresponding to each glass bead concentration across all time points. Data are expressed as mean ± standard deviation (SD)

	Apparent diffusion coefficient ($\mu m^2/ms$)						
	Phantom (glass bead concentration per 30ml)						
	0 g	1.4 g	2.8 g	4.2 g	5.6 g	7.0 g	8.4 g
Day 0	2.06 ± 0.01	1.75 ± 0.01	1.48 ± 0.01	1.31 ± 0.02	1.12 ± 0.01	0.84 ± 0.05	0.65 ± 0.02
Day 30	2.08 ± 0.01	1.76 ± 0.01	1.53 ± 0.01	1.29 ± 0.01	1.05 ± 0.02	0.90 ± 0.03	0.65 ± 0.05
Day 60	2.08 ± 0.01	1.73 ± 0.01	1.52 ± 0.01	1.34 ± 0.02	1.15 ± 0.03	0.89 ± 0.02	0.61 ± 0.04
Day 90	2.06 ± 0.01	1.75 ± 0.01	1.51 ± 0.01	1.30 ± 0.02	1.07 ± 0.03	0.92 ± 0.03	0.57 ± 0.04

Discussion

In this study, we created a phantom composed of CNF and GB and conducted a short-term evaluation of its ADC stability. The present study focused on ADC because ADC is the most widely used quantitative parameter in clinical DWI and was suitable for the initial evaluation of the controllability and temporal stability of the CNF–GB phantom. The phantom was designed to represent isotropic restricted diffusion using spherical glass beads dispersed within the CNF matrix, rather than anisotropic diffusion.

In the phantom without GB (0 g/30 ml), the measured T2 value was 353.6 ms, which is lower than the previously reported T2 values for purified water on 3T MRI systems.[21] The CNF used in this study contained 2 wt% CNFs dispersed—but not dissolved—in purified water. This reduction in T2 is likely due to an increase in water molecules bound to the nanofiber network, leading to restricted molecular motion, a phenomenon similar to what has been reported in agarose gels.[22] In phantoms that included GBs, T2 values declined with increasing GB concentration, a result consistent with expectations since GBs do not contribute to the MR signal.

A strong negative correlation was observed between ADC values and GB density, indicating that water diffusion becomes increasingly restricted as the phantom's internal microstructure becomes more complex. This trend mirrors the commonly reported inverse relationship between ADC and cell density in a variety of tumors,[23-25] demonstrating that our phantom effectively mimics tumor-like diffusion behavior. The observed ADC values ranged from 0.6 to 2.0 $\mu m^2/ms$, aligning with the range typically seen in clinical DWI studies.[26-29] Except for the phantom containing 8.4 g per 30 ml of GB, all other phantoms exhibited ADC CV values below 5%, indicating high short-term stability of the ADC measurements over the 90-day period. These results suggest that the GBs remained evenly distributed within the CNF matrix during the study period, maintaining a consistent microstructural environment suitable for diffusion analysis.

To date, several strategies have been proposed for creating restricted diffusion phantoms incorporating microstructural components such as GBs or acrylic fine particles. These methods include embedding beads within agarose gels, dispersing them in neutral detergent solutions followed by prompt imaging, and adjusting the density of the suspending medium to minimize sedimentation. However, each approach has inherent limitations. Agarose requires a gelation period during which bead settling may occur; suspensions using detergents can result in particle movement during imaging, compromising measurement stability; and density-matching techniques typically involve highly viscous solutions, which are suboptimal since the expected extracellular diffusivity is approximately 2.0$\mu m^2/ms$,[30, 31] similar to that of purified water used in MRI studies.[32, 33] In contrast, the CNF used in this study addressed these limitations effectively. The phantom containing 0 g of GB per 30 ml exhibited an ADC value close to 2.0 $\mu m^2/ms$, approximating extracellular free water diffusion. These results highlight the potential of CNF as a dispersing

agent that not only stabilizes particle suspension but also permits diffusion behavior consistent with physiological conditions. Therefore, the CNF-based phantom represents a novel and practical approach for constructing stable restricted diffusion environments suited for quantitative diffusion MRI validation.

Nonetheless, several limitations should be noted. First, the CNF used in our phantom is also commonly utilized as a food additive, making it vulnerable to biological degradation over time. To reduce the potential impact of microbial spoilage on both the surrounding environment and the diffusion characteristics, we limited the duration of our experiments. Although adding preservatives such as sodium azide might help prevent degradation, the effects of these agents on the structural stability and diffusion behavior of the CNF matrix remain uncertain and require further study. Second, in designing the phantom, we assumed that the restricted diffusion of water molecules was solely influenced by the microstructure of the GBs. However, the CNF network itself may also contribute to diffusion hindrance. To eliminate this potential confounding factor, the phantom containing 0 g/30 ml of GB should be scanned using a range of diffusion times with sequences sensitive to short diffusion times, such as the oscillating gradient spin echo (OGSE) technique.[34-35] If the ADC remains unchanged across different diffusion times, this would support the assumption that CNF has minimal influence on diffusion measurements. It is worth noting that Dan et al. previously demonstrated no diffusion-time dependence of ADC in agarose gel phantoms when assessed using OGSE methods.[36] Nevertheless, because the microstructural properties of CNF differ from those of agarose, the diffusion-time dependence of the CNF matrix should be directly evaluated in future studies. In addition, the diffusion gradient timing parameters, including the δ and Δ, were not available from the vendor-provided clinical single-shot EPI DWI sequence used in this study. Because these parameters determine the effective diffusion time, they may affect ADC values in restricted diffusion environments. Therefore, future studies should use research pulsed-gradient spin-echo or OGSE sequences that allow explicit control or reporting of δ and Δ to evaluate the diffusion-time dependence of the CNF-based phantom. Third, the spatial distribution of glass beads within the CNF matrix was not directly evaluated using CT, optical microscopy, or electron microscopy. We assumed that the dispersion and sedimentation-suppressing properties of CNF would maintain the glass beads in a relatively homogeneous suspension. Although the low ADC coefficients of variation over 90 days indirectly suggest temporal stability of the internal diffusion environment, these results do not directly demonstrate the absence of regional sedimentation or aggregation. Future studies should include direct structural assessment of glass bead distribution and regional ADC analysis along the longitudinal axis of the tube. Fourth, no additional image preprocessing was performed. Specifically, denoising, Gibbs-ringing correction, motion correction, and susceptibility-distortion correction were not applied. The combination of glass beads and CNF may create local magnetic susceptibility differences, and the use of single-shot EPI DWI may result in geometric distortion or signal loss, particularly at higher glass bead concentrations. In the present study, no doping substances or susceptibility-matching agents were used. Although all longitudinal

measurements were performed under identical imaging and analysis conditions, susceptibility-related effects may have influenced the absolute ADC values.

Conclusion

In this study, we successfully developed a new diffusion phantom composed of CNF and GB and evaluated its short-term stability in ADC measurements. The phantom exhibited a broad range of ADC values (0.6−2.0 $\mu m^2/ms$), encompassing the typical range observed in clinical applications. A strong inverse relationship between GB density and ADC was identified, indicating that the phantom effectively replicates diffusion restriction associated with increased microstructural complexity, such as that found in tumors. Notably, ADC values remained stable over a 90-day period, with CVs below 5% in all but the highest GB concentration, demonstrating excellent temporal consistency. These findings show that CNF provides a reproducible diffusion environment without requiring gelation or viscosity modifications. The CNF-based phantom represents a practical, reproducible, and physiologically relevant tool for validating DWI sequences. Its simple preparation and structural stability make it a promising option for standardization and quality control in quantitative DWI.

Statements and Declarations

Competing Interests

The authors declare no competing interests.

Funding

This research did not receive any specific grant from funding agencies in the public, commercial, or not-for-profit sectors.

References

1. Lyng H, Haraldseth O, Rofstad EK. Measurement of cell density and necrotic fraction in human melanoma xenografts by diffusion weighted magnetic resonance imaging. Magn Reson Med 2000; 43 :828-836. https://doi.org/10.1002/1522-2594(200006)43:6%3C828::AID-MRM8%3E3.0.CO;2-P
2. Schnapauff D, Zeile M, Niederhagen MB, Fleige B, Tunn PU, Hamm B, et al. Diffusion-weighted echo-planar magnetic resonance imaging for the assessment of tumor cellularity in patients with soft-tissue sarcomas. J Magn Reson Imaging 2009; 29 :1355-1359. https://doi.org/10.1002/jmri.21755
3. Kishimoto K, Tajima S, Maeda I, Takagi M, Ueno T, Suzuki N, et al. Endometrial cancer: correlation of apparent diffusion coefficient (ADC) with tumor cellularity and tumor grade. Acta Radiol 2016; 57:1021-1028. https://doi.org/10.1177/0284185115612249

4. Liu Y, Ye Z, Sun H, Bai R. Grading of uterine cervical cancer by using the ADC difference value and its correlation with microvascular density and vascular endothelial growth factor. Eur Radiol 2013; 23:757-765. https://doi.org/10.1007/s00330-012-2657-1
5. Santucci D, Faiella E, Calabrese A, Beomonte Zobel B, Ascione A, Cerbelli B, et al. On the Additional Information Provided by 3T-MRI ADC in Predicting Tumor Cellularity and Microscopic Behavior. Cancers (Basel) 2021; 13:5167. https://doi.org/10.3390/cancers13205167
6. Surov A, Gottschling S, Mawrin C, Prell J, Spielmann RP, Wienke A, et al. Diffusion-Weighted Imaging in Meningioma: Prediction of Tumor Grade and Association with Histopathological Parameters. Transl Oncol 2015; 8:517-523. https://doi.org/10.1016/j.tranon.2015.11.012
7. Sakoda K, Baba S. Comparison of apparent diffusion coefficient (ADC) values obtained by echo planar imaging diffusion-weighted imaging (DWI) and radial acquisition regime DWI in low field MRI systems: A phantom study. Radiography (Lond) 2024; 30:1290-1296. https://doi.org/10.1016/j.radi.2024.07.005
8. Laubach HJ, Jakob PM, Loevblad KO, Baird AE, Bovo MP, Edelman RR, et al. A phantom for diffusion-weighted imaging of acute stroke. J Magn Reson Imaging 1998; 8:1349-1354. https://doi.org/10.1002/jmri.1880080627
9. Tofts PS, Lloyd D, Clark CA, Barker GJ, Parker GJ, McConville P, et al. Test liquids for quantitative MRI measurements of self-diffusion coefficient in vivo. Magn Reson Med 2000; 43:368-374. https://doi.org/10.1002/(sici)1522-2594(200003)43:3%3C368::aid-mrm8%3E3.0.co;2-b
10. Maekawa T, Hori M, Murata K, Feiweier T, Fukunaga I, Andica C, et al. Changes in the ADC of diffusion-weighted MRI with the oscillating gradient spin-echo (OGSE) sequence due to differences in substrate viscosities. Jpn J Radiol 2018; 36:415-420. https://doi.org/10.1007/s11604-018-0737-0
11. Amouzandeh G, Chenevert TL, Swanson SD, Ross BD, Malyarenko DI. Technical note: Temperature and concentration dependence of water diffusion in polyvinylpyrrolidone solutions. Med Phys 2022; 49:3325-3332. https://doi.org/10.1002/mp.15556
12. Paudyal R, Konar AS, Obuchowski NA, Hatzoglou V, Chenevert TL, Malyarenko DI, et al. Repeatability of Quantitative Diffusion-Weighted Imaging Metrics in Phantoms, Head-and-Neck and Thyroid Cancers: Preliminary Findings. Tomography 2019; 5:15-25. https://doi.org/10.18383/j.tom.2018.00044
13. Liu YJ, Tsai TS, Li YH, Peng JH, Chang HC, Peng HH, et al. Understanding ADC variation by fat content effect using a dual-function MRI phantom. Eur Radiol Exp 2024; 8:19. https://doi.org/10.1186/s41747-023-00414-0
14. Portakal ZG, Shermer S, Jenkins C, Spezi E, Perrett T, Tuncel N, et al. Design and characterization of tissue-mimicking gel phantoms for diffusion kurtosis imaging. Med Phys 2018; 45:2476-2485. https://doi.org/10.1002/mp.12907

15. Mikayama R, Yabuuchi H, Matsumoto R, Kobayashi K, Yamashita Y, Kimura M, et al. Development of a new phantom simulating extracellular space of tumor cell growth and cell edema for diffusion-weighted magnetic resonance imaging. MAGMA 2020; 33:507-513. https://doi.org/10.1007/s10334-019-00823-6
16. K. Sakoda, S. Baba. Evaluation of the Short- and Long-Term Stability of Apparent Diffusion Coefficient Using the Commercial Product Pseudo-Blood®. Appl Magn Reson 2025; 56:759–768. https://doi.org/10.1007/s00723-025-01754-3
17. Antony Jose S, Cowan N, Davidson M, Godina G, Smith I, Xin J, et al. A Comprehensive Review on Cellulose Nanofibers, Nanomaterials, and Composites: Manufacturing, Properties, and Applications. Nanomaterials (Basel) 2025; 15:356. https://doi.org/10.3390/nano15050356
18. Sharma A, Mandal T, Goswami S. Dispersibility and Stability Studies of Cellulose Nanofibers: Implications for Nanocomposite Preparation. J Polym Environ 2021; 29: 1516–1525. https://doi.org/10.1007/s10924-020-01974-7
19. Wong OL, Yuan J, Zhou Y, Yu SK, Cheung KY. Longitudinal acquisition repeatability of MRI radiomics features: An ACR MRI phantom study on two MRI scanners using a 3D T1W TSE sequence. Med Phys 2021; 48:1239-1249. https://doi.org/10.1002/mp.14686
20. Miquel ME, Scott AD, Macdougall ND, Boubertakh R, Bharwani N, Rockall AG. In vitro and in vivo repeatability of abdominal diffusion-weighted MRI. Br J Radiol 2012; 85:1507-12. https://doi.org/10.1259/bjr/32269440
21. Gatidis S, Schmidt H, Martirosian P, Schwenzer NF. Development of an MRI phantom for diffusion-weighted imaging with independent adjustment of apparent diffusion coefficient values and T2 relaxation times. Magn Reson Med 2014; 72:459-463. https://doi.org/10.1002/mrm.24944
22. Andrasko J. Water in agarose gels studied by nuclear magnetic resonance relaxation in the rotating frame. Biophys J 1975; 15:1235-1243. https://doi.org/10.1016/s0006-3495(75)85896-6
23. Manenti G, Di Roma M, Mancino S, Bartolucci DA, Palmieri G, Mastrangeli R, et al. Malignant renal neoplasms: correlation between ADC values and cellularity in diffusion weighted magnetic resonance imaging at 3 T. Radiol Med 2008; 113:199-213. https://doi.org/10.1007/s11547-008-0246-9
24. Jenkinson MD, du Plessis DG, Smith TS, Brodbelt AR, Joyce KA, Walker C. Cellularity and apparent diffusion coefficient in oligodendroglial tumours characterized by genotype. J Neurooncol 2010; 96:385-392. https://doi.org/10.1007/s11060-009-9970-9
25. Eidel O, Neumann JO, Burth S, Kieslich PJ, Jungk C, Sahm F, et al. Automatic Analysis of Cellularity in Glioblastoma and Correlation with ADC Using Trajectory Analysis and Automatic Nuclei Counting. PLoS One 2016; 11:e0160250. https://doi.org/10.1371/journal.pone.0160250

26. Pi S, Cao R, Qiang JW, Guo YH. Utility of DWI with quantitative ADC values in ovarian tumors: a meta-analysis of diagnostic test performance. Acta Radiol 2018; 59:1386-1394. https://doi.org/10.1177/0284185118759708
27. Tordjman M, Mali R, Madelin G, Prabhu V, Kang SK. Diagnostic test accuracy of ADC values for identification of clear cell renal cell carcinoma: systematic review and meta-analysis. Eur Radiol 2020; 30:4023-4038. https://doi.org/10.1007/s00330-020-06740-w
28. Wang QP, Lei DQ, Yuan Y, Xiong NX. Accuracy of ADC derived from DWI for differentiating high-grade from low-grade gliomas: Systematic review and meta-analysis. Medicine (Baltimore) 2020; 99:e19254. https://doi.org/10.1097/md.0000000000019254
29. Xing H, Song CL, Li WJ. Meta analysis of lymph node metastasis of breast cancer patients: Clinical value of DWI and ADC value. Eur J Radiol 2016; 85:1132-1137. https://doi.org/10.1016/j.ejrad.2016.03.019
30. Reynaud O, Winters KV, Hoang DM, Wadghiri YZ, Novikov DS, Kim SG. Pulsed and oscillating gradient MRI for assessment of cell size and extracellular space (POMACE) in mouse gliomas. NMR Biomed 2016; 29:1350-1363. https://doi.org/10.1002/nbm.3577
31. Jiang X, Li H, Xie J, Zhao P, Gore JC, Xu J. Quantification of cell size using temporal diffusion spectroscopy. Magn Reson Med 2016; 75:1076-1085. https://doi.org/10.1002/mrm.25684
32. Fritz V, Martirosian P, Machann J, Thorwarth D, Schick F. Soy lecithin: A beneficial substance for adjusting the ADC in aqueous solutions to the values of biological tissues. Magn Reson Med 2023; 89:1674-1683. https://doi.org/10.1002/mrm.29543
33. Boursianis T, Kalaitzakis G, Pappas E, Karantanas AH, Maris TG. MRI diffusion phantoms: ADC and relaxometric measurement comparisons between polyacrylamide and agarose gels. Eur J Radiol 2021; 139:109696. https://doi.org/10.1016/j.ejrad.2021.109696
34. Kamimura K, Kamimura Y, Nakano T, Hasegawa T, Nakajo M, Yamada C, et al. Differentiating brain metastasis from glioblastoma by time-dependent diffusion MRI. Cancer Imaging 2023; 23:75. https://doi.org/10.1186/s40644-023-00595-2
35. Ichikawa K, Taoka T, Ozaki M, Sakai M, Yamaguchi H, Naganawa S. Impact of tissue properties on time-dependent alterations in apparent diffusion coefficient: a phantom study using oscillating-gradient spin-echo and pulsed-gradient spin-echo sequences. Jpn J Radiol 2022; 40:970-978. https://doi.org/10.1007/s11604-022-01281-2
36. Wu D, Zhang J. The Effect of Microcirculatory Flow on Oscillating Gradient Diffusion MRI and Diffusion Encoding with Dual-Frequency Orthogonal Gradients (DEFOG). Magn Reson Med 2017; 77:1583-1592. https://doi.org/10.1002/mrm.26242